Desalination and Water Treatment
www.deswater.com

doi: 10.1080/19443994.2013.841109

53 (2015) 543–556
January

Taylor & Francis
Taylor & Francis Group

Adsorptive removal of dye crystal violet onto low-cost carbon produced from Eichhornia plant: kinetic, equilibrium, and thermodynamic studies

Sumanjit Kaur*, Seema Rani, Rakesh Kumar Mahajan

Department of Chemistry, Guru Nanak Dev University, Amritsar 143005, India
Tel. +91 183 2256818; Fax: 91 183 2258820; email: sumangndu@yahoo.co.in

Received 21 June 2013; Accepted 20 August 2013

ABSTRACT

Eichhornia charcoal is used as a potential adsorbent to remove dye crystal violet (CV) from aqueous solutions. Material was characterized for its surface chemistry by elemental analysis, Boehm titrations, point of zero charge measurements, Brunauer–Emmett–Teller, scanning electron microscopy, Fourier transform infrared spectroscopy, and X-ray diffraction. Adsorption conditions were optimized by considering the effect of contact time, pH, initial concentration of the dye, and temperature. It is surmised that adsorption of CV increases with increase in pH, temperature, amount of adsorbent, ionic strength, and contact time. The equilibrium adsorption data were analyzed by Langmuir, Freundlich, Temkin, Dubinin and Radushkevich and generalized isotherms models. Adsorption kinetics were contemplated using pseudo-first order, pseudo-second order, intraparticle diffusion, Elovich model, and Bangham's model. Equilibrium adsorption of CV was better explained by Langmuir adsorption model and evidenced the maximum adsorption capacity as 58.13 mg g^{-1}. Higher coefficient of determination ($R^2 > 0.99$) and better agreement between the $q_{e,cal}$ and $q_{e,exp}$ values suggested that pseudo-second-order kinetic model better represents the kinetic adsorption data with rate constant 0.011, 0.015, and 0.024 g mg^{-1} min^{-1} at 303, 313, and 323 K, respectively. The energy of activation for the present system was found to be 31.82 kJ mol^{-1}. Thermodynamic parameters manifested that adsorption process is spontaneous and endothermic in nature.

Keywords: Eichhornia; Crystal violet; Adsorption; Kinetics; Isotherm

1. Introduction

Crystal violet (CV) is also known as basic violet 3, gentian violet, and methyl violet 10B. Its IUPAC name is N-[4-[bis[4-dimethylamino)phenyl]methylene]- 2,5-cyclo hexadien-1-ylidine]-N-methyl methanaminium chloride and belongs to the class of triarylmethane dyes. CV is used as a pH indicator (yellow to violet with the transition at a pH 1.6). In the medical community, it is the active ingredient in Gram's stain and is employed as a bacteriostatic agent [1]. It is also used for various purposes such as a biological stain, a dermatological agent, a veterinary medicine, an additive to poultry feed to inhibit propagation of mold, intestinal parasites and fungus. It is extensively used in textile dying and paper coloration. It is a mutagen and mitotic poison [2]. CV is a protein dye and hence acts as an enhancer for bloody fingerprints. CV is carcinogenic and has been classified as a recalcitrant molecule, since

---

*Corresponding author.

it is poorly metabolized by microbes, is non-biodegradable, and can persist in a variety of environments. The dye is responsible for causing moderate eye irritation, causing painful sensitization to light. It can also cause permanent injury to the cornea and conjunctiva, since the product contains a cationic dye. It is highly toxic to mammalian cells and if absorbed in harmful amounts through the skin, it can cause skin irritation and digestive tract irritation. In extreme cases, it may also lead to respiratory and kidney failures [1,3,4]. Hence, the CV removal from the water bodies becomes essential.

Various treatments for the removal of dyes including aerobic and anaerobic microbial degradation, coagulation, chemical oxidation, membrane separation, electrochemical treatment, filtration, flocculation, softening, hydrogen peroxide catalysis, and reverse osmosis have been studied recent years [5,6]. However, these processes have disadvantages and limitations of high cost, generation of secondary pollutants and poor removal efficiency [7]. Thus, adsorption has been found to be an effective and attractive process for the treatment of dye-containing wastewaters. Adsorption is a well-known and superior technique for dye and organic removal because of its easy operation, insensitivity to toxic substances, ability to treat concentrated forms of the dyes, and the possibility of reusing the spent adsorbent via regeneration. Consequently, the commercially available activated carbon is in use. Since a large amount of carbon adsorbent is needed for the removal of dyes from a large volume of effluent, the expenses involved hamper their application [8]. In recent years, many studies have focused on seeking cheap, locally available and effective adsorbents for the removal of dyes. A large number of industrial and agricultural waste materials have been successfully utilized by various workers as potential adsorbents for the removal of dyes from water and wastewater [1,6,9–19].

In the present study, *Eichhornia crassipes* are used as an adsorbent, as it is available in plenty and people have been trying to remove the plant from many water ways, spending billions of dollars in doing so. *E. crassipes* (water hyacinth) has invaded many tropical lakes, including Lake Victoria, adversely affecting fisheries, transportation, and hydroelectric power production. It is blamed for providing favorable conditions for breeding of snails, mosquitoes and snakes. Eichhornia is available plenty in India and also considered as one of the worst weed in the world. *E. crassipes* (Water hyacinth) is a free floating aquatic plant well known for its production abilities and removal of pollutants from water [20]. It is vigorous grower known to double their population within two weeks. Large dense *E. crassipes* mat can degrade water quality and can choke water way. This article is aimed to study a convenient and economic method for CV removal from water by adsorption on charcoal derived from *E. crassipes*; to gain an understanding of the adsorption kinetics; to describe the rate and mechanism of adsorption; to determine the factors controlling the rate of adsorption; to calculate the thermodynamic parameters and activation energy of the system. The adsorption models were applied to describe the equilibrium isotherms and corresponding isotherm constants were determined.

2. Materials and methods

Eichhornia collected from a pond at Ram Tirath Road, Amritsar, was washed several times with normal tap water followed by distilled water to remove adhered dust particles and impurities. It were dried in the sun for 2 weeks and then in oven at 60˚C for 12 h. The cleaned material was ground to fine material then carbonized at 600˚C at the rate of 10˚C per minute. After carbonization, the adsorbent (Eichhornia charcoal, EC) was cooled and sieved through sieves having mesh number 270 to remove coarse particles, and the corresponding particle size of 53 μm was obtained [21] and then kept in desiccators before use.

CV (Molecular formula: $C_{25}H_{30}N_3Cl$, M.W.: 407.98, C.I. no. 42,555, $\lambda_{\max} = 580$ nm) was purchased from SD-fine chemicals and used as such. Stock solution of dye was prepared by dissolving 1 g of dye in 1,000 mL of double-distilled water to give the concentration of 1,000 mg L^{-1}. The stock solution was diluted to known initial concentrations.

2.1. Characterization of adsorbent

Fourier transform infrared (FTIR) spectra of the samples were recorded between 4,000 and 500 cm^{-1} using a Perkin–Elmer FTIR spectrometer. One centimeter diameter and constant weight KBr pellets were prepared by mixing the samples with KBr at 1:5 ratio, and oven-dried 48 h at 110˚C before analysis. The materials are further characterized by using the X-ray diffraction (XRD) in the scanning mode on an XRD 7000 (Shimadzu, Japan) analytical instrument operated at 40KV and a current of 30 mA with Cu-Kα radiation (λ = 1.5406 Å). Scanning electron microscopy (SEM) observations of the EC and dye-loaded EC were carried out using a scanning microscope (Carl Zeiss Supra 55), equipped with EDX analyzer, and analysis was carried out by gold-sputtering process to avoid charging under the electron beam.

The N_2 adsorption–desorption isotherms of the adsorbent was measured using an automatic adsorption instrument (Micromeritics Chemisorb 2720) at liquid nitrogen temperature (77 K). Prior to measurements, sample was degassed at 300˚C for 12 h under vacuum. The specific surface area (SBET) of the adsorbent was calculated using the Brunauer–Emmett–Teller (BET) equation by assuming the area of the nitrogen molecule to be $0.162\,nm^2$. The total pore volumes were estimated from the liquid volume of adsorbate adsorbed (N_2) at a relative pressure of 0.99. In addition, the pore size distribution was determined by using the Barrett–Joyner–Halenda method applied on the adsorption/desorption hysteresis loop assuming a model of cylindrical open-ended pores. Particle size was determined by particle size analyzer (Ankersmid CIS100).

The pH of adsorbent was measured in a distilled water suspension (50 mL) of 0.5 g of adsorbent after heating at 90˚C and then cooling to room temperature. The pH of zero point charge (pH_{zpc}) plays an important role in the adsorption process. The pH_{zpc} of adsorbent EC was determined by the method reported already [22]. For this purpose, 50 mL of a 0.01 M sodium chloride (NaCl) solution was placed in a 100-mL Erlenmeyer flask. The pH was adjusted to successive initial values between 2 and 12, by using either sodium hydroxide or hydrogen chloride (0.1 N), and 0.15 g of adsorbent was added to the solution. After a contact time of 24 h, the final pH was measured and plotted against the initial pH. The pH at which the curve crosses the line pH (final) = pH (initial) is taken as the pH_{zpc}. The pH of the EC was also measured in distilled water suspension.

Surface chemistry was determined using Boehm titration methods [23]. Boehm titrations quantify the basic and oxygenated acidic surface groups on activated carbons. In this study, surface functional groups such as carboxyl (R–COOH), lactone (R–OCO), phenol (Ar–OH), carbonyl or quinone (RR´C=O) and basic groups were determined. Sodium ethoxide ($NaOC_2H_5$), sodium hydroxide (NaOH), sodium carbonate (Na_2CO_3), and sodium hydrogen carbonate ($NaHCO_3$) were used as basic reagents. Surface functional groups were quantified by assuming that $NaOC_2H_5$ reacted with all groups; NaOH did not react with the RR´C=O groups; Na_2CO_3 did not react with RR´C=O and R–OH groups; and that $NaHCO_3$ only reacted with R–COOH groups. The adsorbent was also titrated by hydrochloric acid (HCl) in order to estimate the amount of bases within the material.

Experimentally different batches of 100 mg adsorbent was brought into contact with 50 mL solutions of 0.01 M $NaHCO_3$, 0.01 M Na_2CO_3, 0.01 M NaOH, and 0.01 M HCl. The mixtures were retained in a mechanical agitator at 100 rpm and 25˚C for 24 h. Then, the aliquots were back-titrated with either 0.01 M HCl for acidic groups or 0.01 M NaOH for basic groups. The amount of each functional group was calculated with the assumptions that $NaHCO_3$ neutralizes only carboxylic groups, Na_2CO_3 neutralizes carboxylic and lactonic groups, and NaOH neutralizes carboxylic, lactonic, and phenolic groups, while HCl neutralizes basic groups [23].

2.2. Adsorption experiments

Batch adsorption experiments were conducted in 250-mL shaker flasks containing 50 mL aqueous solution with known dye concentration (adjusted to the desired pH with 0.1 M NaOH/HCl) and 50 mg of adsorbent. For each test, the mixture was agitated for equilibrium time at 130 rpm in a thermostated metrex water bath orbital shaker. Aliquots were withdrawn at different time intervals and filtered using Whatmann filter paper (no. 41). The supernatants were used for dye concentration analysis. All the dye adsorption experiments were conducted in triplicate, and the average values were recorded.

The amount of dye adsorbed per unit EC (mg dye per g adsorbent) was calculated according to a mass balance on the dye concentration using equation: $q_t = V\ (C_o - C_t)/M$ where C_o is the initial dye concentration ($mg\,L^{-1}$), C_t is the dye concentration in solution ($mg\,L^{-1}$) at time t, V is the volume of the solution (L), and M is the mass of the adsorbent (g). The percent removal (%) of dye was calculated using the equation: $\text{Removal}\ (\%) = ((C_o - C_e)/C_o) \times 100$

Where C_e is the concentration of dye solution ($mg\,L^{-1}$) at equilibrium. Microsoft Excel program was employed for data processing. Linear regression analyses were used to determine slopes and intercepts of the linear plots and for statistical analyses of the data.

3. Results and discussion

3.1. pH, pH_{zpc}, surface functional group, and element analysis

pH of the material suspension, pH_{zpc} as well as oxygenated group contents analyzed by titration are 8.0, 7.9, and $0.034\,mmol\,g^{-1}$, respectively, whereas total basic group was found to be $0.047\,mmol\,g^{-1}$. The basic nature of the adsorbent enhanced the adsorption of cationic dye CV. The value of pH is similar to pH_{zpc} indicating the basic nature of adsorbent EC. EC contains mainly carbon (30%), nitrogen (2.5%), and hydrogen (1.64%). Particle size, total pore volume, monolayer volume, cross sectional area, and BET surface area obtained were 0.45–51 µm, 0.012 $m^2 g^{-1}$, 5.42 $cm^3 g^{-1}$, 0.16 nm^2, and 23.63 $m^2 g^{-1}$, respectively.

3.2. FTIR study

FTIR technique was used to examine the surface groups of the adsorbent and to identify the groups responsible for dye adsorption. Spectra of dye CV having peak values at 3,215, 1,583, 1,479, 1,363, 1,294, and 1,171 cm^{-1}. The value at 3,215 cm^{-1} may be due to –OH group, region between 1,475 and 1,600 is due to C=C (aromatic), and 1,350–1,000 cm^{-1} for C–N stretching. The sharp peak at 1,585 cm^{-1} indicates the presence of aromatic ring. Adsorbent EC shows peaks mainly at 3,378 (H bonded OH stretching), 1,605 (aromatic ring), 1,418, 1,316, and 1,032 cm^{-1}. The strong band at 1,309 cm^{-1} indicates Si–O linkage. Region of 1,300–1,000 cm^{-1} is for C–O stretching. When dye molecules get loaded on the surface of adsorbent the intensity of the values get shifted to low frequency region as shown in Fig. 1. The sharp peak at 1,363 cm^{-1} of dye molecule due to C–N stretching disappears in dye-loaded adsorbent.

3.3. XRD study

XRD technique is a powerful technique to analyze the crystalline and amorphous nature of the material under investigation. In crystalline material, well-defined peaks are observed, whereas in noncrystalline or amorphous material shows broad peaks instead of sharp peaks. Fig. 2 shows that well-defined peaks are observed for the adsorbent EC, which indicates that EC is crystalline in nature. There is no significant difference for XRD profiles, but dye-loaded EC sample presents higher intensity of diffraction peaks as compare to unloaded adsorbent. XRD crystallite size is calculated using Scherrer formula [24], $D = K\ \lambda/\beta \cos\theta$, where K is the shape factor, λ is the X-ray wavelength, β is the line broadening at half the maximum intensity (FWHM) in radians, and θ is the Bragg angle. The dimensionless shape factor, K, has a typical value of 0.9, but varies with the actual shape of the crystallite. Peak width is inversely proportional to crystallite size, and results show that as crystallite size get smaller, peak get broader. Peak intensity is usually weakest at large angle 2 θ. Crystallite size at maximum intensity was found to be 42.4 nm for EC. Similar method was adopted by other workers [25] to calculate the average size of the particles.

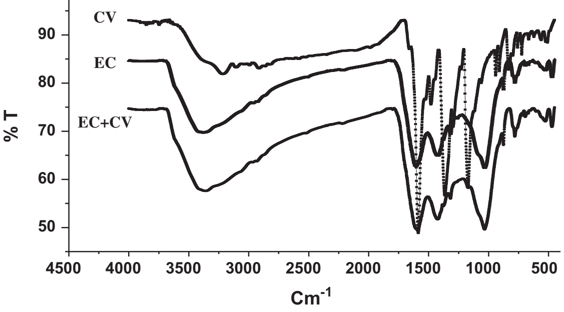

Fig. 1. FTIR spectra of CV, EC, and dye-loaded EC.

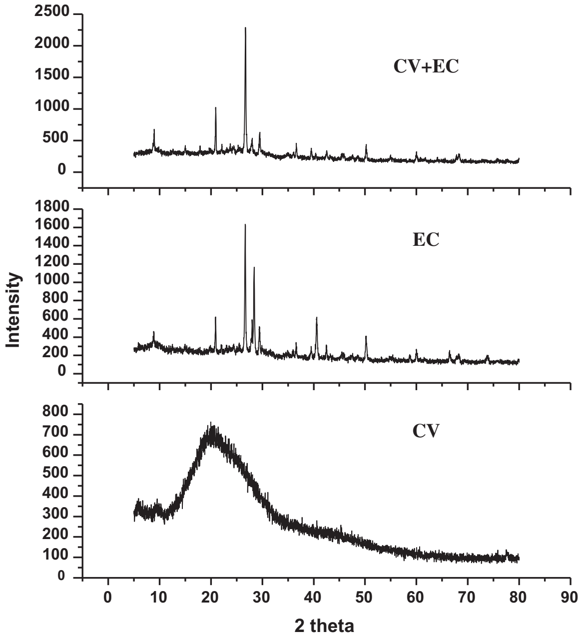

Fig. 2. XRD spectra of CV, EC, and dye-loaded EC.

3.4. SEM study

The morphology and structure of adsorbent surface are characterized using SEM. SEM images of adsorbent before adsorption, after adsorption, clearly indicates the surface texture, and porosity of the EC adsorbent Fig. 3(A) and pores of the adsorbent get loaded by dye molecules Fig 3(B). The analysis of images showed the height of heterogenous pores within EC particles where adsorption could occur. After adsorption, the pores were packed with dye molecules.

3.5. pH influence

The effect of pH on dye adsorption was investigated at 313 K with 20 $mg L^{-1}$ dye solution and 1 $g L^{-1}$

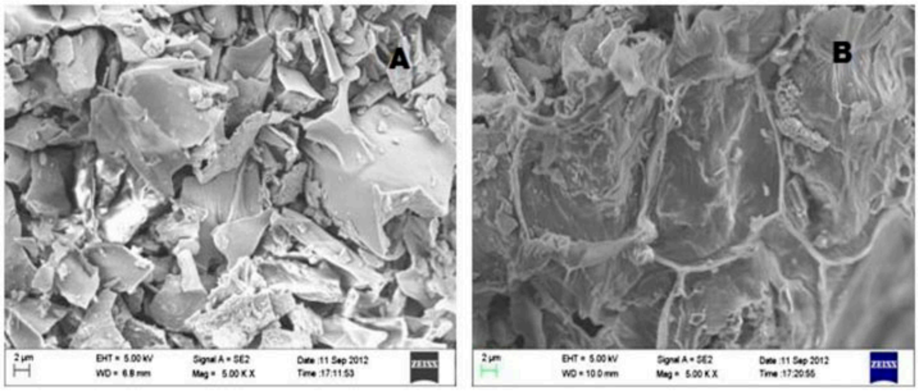

Fig. 3. SEM for (A) EC (B) EC adsorbed with CV.

adsorbent. The results obtained are shown in Fig. 4. The pH of the adsorbent in aqueous solution was found to be 8.0. Adsorption of cation is favored at $pH > pH_{ZPC}$, while the adsorption of anion is favored at $pH < pH_{ZPC}$ [26]. The pH_{ZPC} value for EC was found to be 7.9, respectively. The pKa of CV is 0.8; it is completely ionized at pH greater than 0.8 and exists as cationic species [27]. At low pH (pH = 2), adsorptive removal was found to be 73%, and at high pH, the removal was 95%. At low pH values, protonation of the functional groups present on the adsorbent surface takes place. The surface of the adsorbent becomes positively charged, and this decreases the adsorption of the positively charged dye ions through electrostatic repulsion. However, as the pH of the dye solution increases, a considerable increase in dye-binding capacity is observed due to strong electrostatic attraction between negatively charged sites on the adsorbent and the dye cations. With further increase in pH has no significant effect. Basic conditions favor the adsorption of dye, and hence, pH 8.0 was considered as optimum pH for the adsorption of the dye.

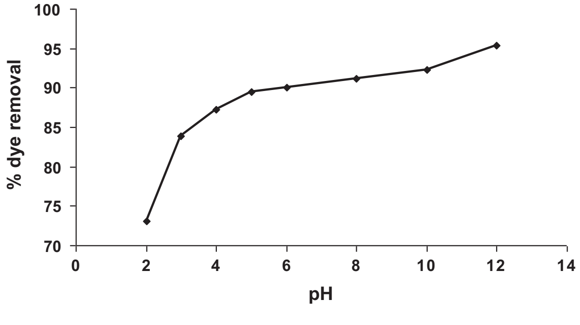

Fig. 4. Effect of pH on the adsorption of CV onto EC at 313 K. (adsorbent dose = 1 g L^{-1}, C_o = 20 mg L^{-1}, equilibrium time = 150 min).

3.6. Effect of the contact time and of the initial dye concentration

The contact time is one of the factors for the development of surface charges at the solid–solution interface [28]. The variation of percentage of dye adsorbed with respect to time is shown in Fig. 5(a). Curves show that dye removal increases with time. The initial rate was rapid, and thereafter, it was gradual until the

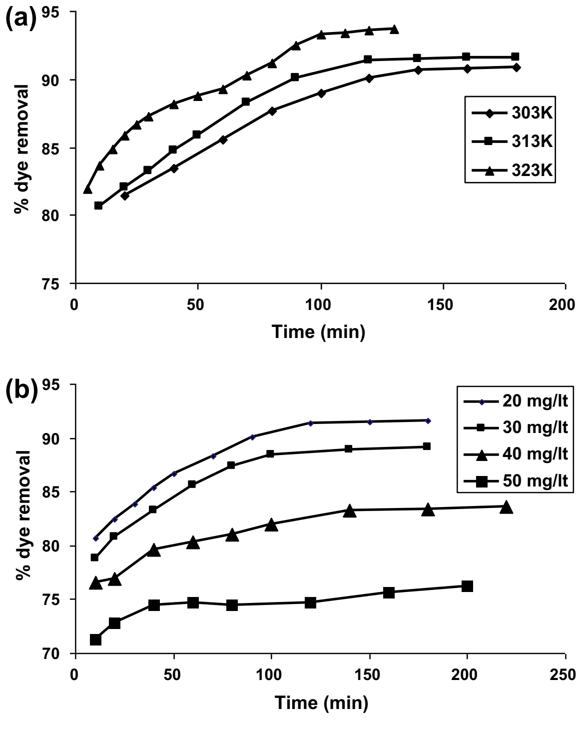

Fig. 5. (a) Effect of contact time on the adsorption of CV onto EC at different temperatures. (adsorbent dose = 1 g L^{-1}, C_o = 20 mg L^{-1}, pH = 8.0). (b) Effect of contact time on the adsorption of CV onto EC at different concentrations. (adsorbent dose = 1 g L^{-1}, pH = 8.0, T = 313 K).

equilibrium was reached. The initial stage indicates rapid attachment of CV molecules to the external surface of the EC followed by slow percentage removal due to diffusion of solute molecules into pores of the adsorbent or other surface reactions and then final equilibrium stage [29]. The equilibrium time at 303, 313, and 323 K was found to be 180, 150, and 120 min, respectively.

Fig. 5(b) illustrated that percentage dye removal increases from 76 to 91% by decreasing the initial concentration of dye CV from 50–20 mg L^{-1}. Similar results were reported by other workers [17]. However, in the first 30 min, the initial rate of adsorption was greater for higher initial concentration is due to acceleration of the diffusion of dyes from the dye solution onto adsorbent due to the increase in the driving force of the concentration gradient [30].

3.7. Effect of adsorbent dose

Fig. 6 illustrates the removal of dye CV as a function of EC dosage. The number of available adsorption sites increases by increasing the adsorbent dose and it, therefore, results in the increase of the amount of adsorbed dye. The initial rise in adsorption with adsorbent dose is probably due to a stronger driving force and larger surface area. The decrease in adsorption density with increase in the adsorbent dose is mainly because of unsaturation of adsorption sites through the adsorption process [31,32]. Another reason may be due to the particle interaction, such as aggregation, resulting from high adsorbent dose. Such aggregation would lead to decrease in total surface area of the adsorbent and an increase in diffusional path length [31].

3.8. Effect of salt

The effect of salt (NaCl) on adsorption was investigated to study the interactions of salts with adsorbent and adsorbate. Fig. 7 shows that addition of small quantity (0.01 M) of salt of dye increases the dye adsorption. Theoretically, when the electrostatic forces between the adsorbent surface and adsorbate ions were attractive, an increase in ionic strength will decrease the adsorption capacity. Conversely, when the electrostatic attraction is repulsive, an increase in ionic strength will increase adsorption [33,34]. The significant increase in dye removal can be attributed to an increase in dimerization of cationic dyes in solution. A number of intermolecular forces have been suggested to explain this aggregation, these forces include: van der Waals forces; ion dipole forces; and dipole dipole forces, which occur between dye molecules in the solution. It has been reported that these forces increased upon the addition of salt to the dye solution [34], i.e. salt ions force dye molecules to aggregate, increasing the extent of sorption on the adsorbent surface.

3.9. Equilibrium isotherms for CV

The equilibrium isotherms describe how the adsorbent interacts with the adsorbate. The correlation of experimental results to adsorption model can help to understand the mechanisms of adsorption and the heterogeneity of the adsorbent surface, and it is also of importance in the practical design and operation of adsorption.

3.9.1. Langmuir Isotherm

The Langmuir isotherm is based on the existence of monolayer coverage of the adsorbate at the outer surface of the adsorbent, once an adsorbate molecule occupies a site, no further adsorption can take place at that site. Adsorption takes place at specific homogeneous sites within the adsorbent, where all sorption sites are identical and energetically equivalent.

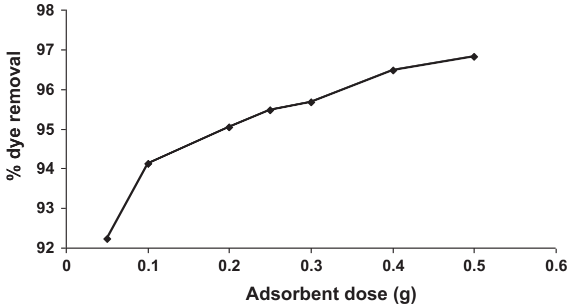

Fig. 6. Effect of adsorbent dose on the adsorption of CV onto EC at 313 K. ($C_o = 20$ mg L^{-1}, pH = 8.0, equilibrium time = 150 min).

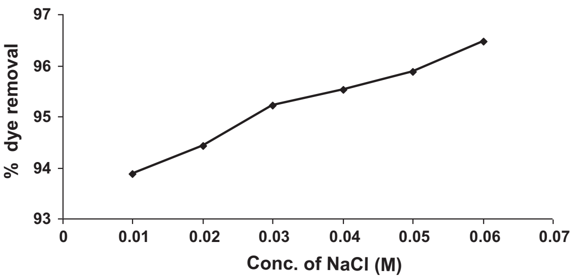

Fig. 7. Effect of salt concentration on the removal of dye CV EC at 313 K. ($C_o = 20$ mg L^{-1}, sorbent dose = 1 g L^{-1}, pH = 8.0, equilibrium time = 150 min).

The linear equation can be expressed as follows:

$$C_e/q_e = C_e/C_m + 1/K_L C_m \tag{1}$$

where C_e is the concentration of dye solution (mg L^{-1}) at equilibrium and q_e (mg g^{-1}) is the adsorption capacity at equilibrium. The constant C_m (mg g^{-1}) signifies the maximum monolayer adsorption capacity of dye CV, which depends on the number of adsorption sites and K_L is related to the affinity of the binding sites. The isotherm parameters calculated from the linear relation between C_e/q_e and C_e are also presented in Table 1.

The Langmuir adsorption constant K_L (L mg^{-1}) can be used to determine a dimensionless separation factor R_L, defined by following equation:

$$R_L = 1/(1 + K_L C_o) \tag{2}$$

where C_o is the initial dye concentration (mg L^{-1}). The value of parameter R_L indicates the nature of the adsorption process. (i) $R_L > 1$ for unfavorable adsorption, (ii) $R_L = 1$ for linear adsorption, (iii) $0 < R_L < 1$ for favorable adsorption, and (iv) $R_L = 0$ for irreversible adsorption. R_L value decreased with the increase in C_o. The R_L values attained are 0.15, 0.13, and 0.12 at 303, 313, and 323 K, respectively at initial dye concentration 20 mg L^{-1}. Values of R_L are greater than zero and less than unity, and it shows that Langmuir isotherm is favorable for the adsorption of CV on EC.

3.9.2. Freundlich isotherm

The Freundlich isotherm is commonly used for investigating the nonlinear adsorption of a variety of dyes on various materials. The Freundlich isotherm is an empirical equation assuming that the adsorption process takes place on heterogeneous surfaces, and adsorption capacity is related to the concentration of dye at equilibrium.

$$\log x/m = \log K_F + 1/n \log C_e \tag{3}$$

where q_e is the amount adsorbed (mg g^{-1}), and C_e is the equilibrium concentration of the adsorbate (mg L^{-1}). K_F (mg g^{-1}) (L g^{-1})$^{1/n}$ and n, the Freundlich constants, are related to adsorption capacity and adsorption intensity, respectively. Value of K_F is increased with increasing temperature, thereby indicating an increased dye–adsorbent interaction at higher temperature. Value of n greater than one reflected that Freundlich model is applicable to the present system in the studied concentration range. Values of K_F and n obtained from the slope and intercept of the plot log q_e vs. log C_e (not shown) are given in Table 1.

3.9.3. Tempkin isotherm

The Temkin isotherm contains a factor that explicitly takes into account the adsorbing species–adsorbent interactions. This isotherm assumes that: (i) the heat of adsorption of all the molecules in the layer decreases linearly with coverage due to adsorbent–adsorbate interactions and that (ii) the adsorption is characterized by a uniform distribution of binding energies, up to some maximum binding energy [35]. The linear form of this isotherm can be given by:

$$q_e = B_1 \ln K_T + B_1 \ln C_e \tag{4}$$

where $B_1 = (\mathrm{RT})/b_T$, T (K) is the absolute temperature, and R is the universal gas constant (8.3145 J mol^{-1} K^{-1}). The constant b_T is related to the heat of adsorption, and K_T is the equilibrium binding constant corresponding to the maximum binding energy. The values of B_1, and K_T obtained from the graphical plot of q_e vs. ln C_e are contained in Table 1.

3.9.4. Dubinin and Radushkevich Isotherm

Dubinin and Radushkevich (D–R) isotherm assumes monolayer adsorption in the micropores of the adsorbent. The linear form can be given as [36].

$$\ln q_e = \ln q_s - B\epsilon^2 \tag{5}$$

where q_s is D–R constant and $\in$ can be correlated as:

$$\epsilon = RT \ln(1 + 1/C_e) \tag{6}$$

where q_s (mg g^{-1}) is the maximum amount of adsorbate that can be adsorbed on adsorbent, the constant B gives the mean free energy E of sorption per molecule of sorbate when it is transferred to the surface of the solid from the bulk solution and can be computed using the following relationship:

$$E = 1/(2B)^{1/2} \tag{7}$$

The calculated D–R constant are provided in Table 1. Mean adsorption energy calculated from D–R isotherm gives an idea about the chemisorptions or physisorption. For $E < 8$ kJ mol^{-1}, physisorption control the adsorption mechanism, while a value between 8 and 16 kJ mol^{-1} indicates involvement of chemisorptions process [37]. The values of E in the present system demonstrated that adsorption of CV on EC is physical in nature.

3.9.5. Generalized Isotherm:

The generalized Isotherm has been used in the following form [38].

$$\ln[(q_{\max}/q_e) - 1] = \ln K_G - N \ln C_e \tag{8}$$

where K_G is the saturation constant (mg L^{-1}), N is the cooperative binding constant, $q_{\max}$ is the maximum adsorption capacity of the adsorbent (mg g^{-1}). q_e (mg g^{-1}) and C_e (mg L^{-1}) are the equilibrium dye concentrations in the solid and liquid phase, respectively. The values of N and K_G are calculated from the slope and intercept of the plots given in Table 1. Saturation constant decreases with increase in temperature may be ascribed to speedy saturation at higher temperature.

3.10. Kinetics study

Adsorption kinetics is an important parameter for designing adsorption systems and is required for selecting optimum operating conditions for batch adsorption study. Different kinetic models along with correlation coefficients (R^2) were used to describe the CV adsorption onto EC.

3.10.1. First-order model

The pseudo-first-order equation is given as:

$$\frac{dq_t}{dt} = k_f(q_e - q_t) \tag{9}$$

where q_t (mg g^{-1}) is the amount of dye adsorbed at time t. q_e (mg g^{-1}) is the adsorption capacity at equilibrium, k_f (min^{-1}) is the pseudo-first-order rate constant, and t is the contact time (min). The integration of Eq. (9) with initial condition ($q_t = 0$ at $t = 0$) leads to following equation:

$$\log(q_e - q_t) = \log q_e - \frac{K_f}{2.303} t \tag{10}$$

The values of pseudo-first-order rate constants, k_f and q_e were calculated from slopes and intercepts of the plots of log ($q_{e\,-}\,q_t$) vs. t and are listed in Table 2. The q_e values calculated from this rate model does not agree well with q_e (experimental) values. It implies that adsorption does not follow first order kinetic model.

3.10.2. Second-order model

The pseudo-second-order model is represented as:

$$\frac{dq_t}{dt} = k_s(q_e - q_t)^2 \tag{11}$$

Table 1
Isotherm parameters for the removal of CV onto EC at different temperatures (adsorbent dose = 1 g L^{-1}, Co = 20 mg L^{-1}, equilibrium time = 150 min, pH = 8)

Equations	Parameters	Temperature (K)		
		303 K	313 K	323 K
Langmuir	K_L (L mg^{-1})	0.29	0.33	0.36
	C_m (mg g^{-1})	50.50	52.91	58.13
	R^2	0.96	0.99	0.96
Freundlich	K_F (mg g^{-1}) (L mg^{-1})$^{1/n}$	11.03	12.87	15.25
	n	1.24	1.25	1.23
	R^2	0.98	0.99	0.99
Tempkin	K_T(L mg^{-1})	4.38	5.25	6.35
	B_1	8.05	8.22	8.31
	R^2	0.98	0.98	0.96
D–R	q_s(mg g^{-1})	18.38	19.28	19.57
	E (kJ mol^{-1})	2.23	2.23	2.5
	R^2	0.96	0.93	0.94
Generalized	N	1.01	1.00	0.99
	K_G(mg L^{-1})	3.47	3.03	2.79
	R^2	0.99	0.99	0.99

where k_s is the pseudo-second-order rate constant (g mg^{-1} min^{-1}). Integrating Eq. (11) ($q_t = 0$ at $t = 0$), the following equation is obtained.

$$\frac{t}{q_t} = \frac{1}{k_s q_e^2} + \frac{1}{q_e} t \tag{12}$$

where k_s is the pseudo-second-order rate constant (g mg^{-1} min^{-1}), and q_e is the equilibrium sorption uptake at time t = infinity. The pseudo-second-order model is generally reported to predict the behavior over the entire range of the adsorption process. The values of q_e and k_s can be obtained from the slope and intercepts of the t/q_t vs. t plots and are given in Table 2. Results surmised that the value of k_s increases with increase in temperature. The correlation coefficient (R^2) values for the pseudo-second-order equation are 0.99. The value of correlation coefficient for pseudo-second-order kinetic model is relatively high than pseudo-first-order and the q_e calculated from the model are closer to those determined experimentally. Therefore, it is concluded that pseudo-second-order kinetic model is more suitable for explaining the adsorption kinetics of dye CV on EC.

3.10.3. Weber–Morris intraparticle diffusion equation

Intraparticle diffusion equation was used to study diffusion mechanism and to determine intraparticle diffusion rate constant (k_{id}). An empirically found functional relationship common to most adsorption process is that the uptake varies almost proportionally with $t^{½}$, the Weber–Morris plot (q_t vs. $t^{1/2}$), rather than with the contact time, t [39].

$$q_t = k_{id} t^{1/2} + C \tag{13}$$

k_{id}, the intraparticle diffusion rate constant (mg/g min$^{0.5}$) can be obtained from the slope of the q_t vs. $t^{1/2}$ plot and is listed in Table 2. Value of C gives an idea about the thickness of the boundary layer, i.e. the larger the intercept, the greater is the boundary layer effect. If the Weber–Morris plot of q_t vs. $t^{1/2}$ satisfies the linear relationship with the experimental data, then the sorption process is found to be controlled by intraparticle diffusion only. However, if the data exhibit multilinear plots, then two or more steps influence the sorption process. The first, sharper portion is attributed to the diffusion of adsorbate through the solution to the external surface of adsorbent or boundary layer diffusion of solute molecules. The second, linear portion is the gradual equilibrium stage with intraparticle diffusion dominating. The third portion is attributed to the final equilibrium stage for which the intraparticle diffusion starts to slow down due to the extremely low adsorbate concentration left in the solution [40]. In the present study the plots do not pass through the origin, this is indicative of some degree of boundary layer control and it shows that the intraparticle diffusion is

Table 2
Kinetic parameters for the adsorption of CV onto EC at different temperatures (adsorbent dose = 1 g L^{-1}, C_o = 20 mg L^{-1}, equilibrium time = 150 min, pH = 8)

Equations	Parameters	Temperature (K)		
		303 K	313 K	323 K
Pseudo first order	q_e exp (mg g^{-1})	18.03	18.16	18.57
	q_e cal (mg g^{-1})	6.29	3.82	2.59
	k_f (min^{-1})	0.031	0.026	0.021
	R^2	0.83	0.97	0.97
Pseudo-second-order	q_e exp (mg g^{-1})	18.03	18.16	18.57
	q_e cal (mg g^{-1})	18.51	18.55	18.72
	k_s (g mg^{-1} min^{-1})	0.011	0.015	0.024
	R^2	0.99	0.99	0.99
Intra-particle diffusion	k_{id} (mg/g min$^{0.5}$)	0.24	0.26	0.28
	C (mg g^{-1})	15.00	15.06	15.61
	R^2	0.97	0.95	0.98
Elovich	a	2.75×10^5	8.88×10^5	15.44×10^7
	b	0.97	1.03	1.30
	R^2	0.96	0.94	0.96
Bangham	k_o (g)	89.80	98.46	123.62
	α	0.18	0.17	0.14
	R^2	0.95	0.93	0.93

not the only rate-limiting step, but also other kinetic models may control the rate of adsorption, all of which may be operating simultaneously.

To exactly deduce the experimental findings, sorption data were given a quantitative treatment based on the model proposed by Richenberg [41], and various parameters were calculated by using the following equations:

$$F = 1 - \frac{6}{\Pi^2}\exp(-\mathrm{Bt}) \tag{14}$$

where F is the fractional attainment of equilibrium at time "t", and Bt is a mathematical function of F. The F (fractional attainment) is acquired by applying following equation:

$$F = \frac{q_\mathrm{t}}{q_\mathrm{e}} \tag{15}$$

where q_t (mg g^{-1}) and q_e(mg g^{-1}) are amounts adsorbed after time t and at equilibrium time, respectively. Substituting Eq. (15) into Eq. (14), the kinetic expression becomes:

$$\mathrm{Bt} = -0.4977 - \ln\left(1 - \frac{q_\mathrm{t}}{q_\mathrm{e}}\right) \tag{16}$$

From the plot of Bt vs. time (Fig. 8), the process was classified as a film diffusion or particle diffusion-controlled mechanism. If a plot of Bt vs. t is a straight line passing through the origin, then adsorption will be governed by a particle-diffusion mechanism, otherwise governed by film diffusion [42]. From Fig. 8 and it is observed that the plot has not a desirable linear form ($R^2 = 0.85$) at 303 K which indicates the ongoing adsorption processes to be governed by film diffusion mechanism, whereas at high temperature 313 and 323 K, plots having linear form with $R^2 = 0.97$, suggesting adsorption process as particle diffusion at high temperature.

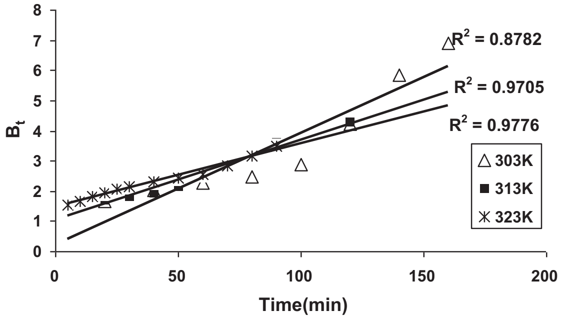

Fig. 8. Correlationship of Bt vs. time (min) on the adsorption of CV onto EC at different temperatures. (adsorbent dose = 1 g L^{-1}, C_o = 20 mg L^{-1}, pH = 8.0).

3.10.4. Elovich model

The most interesting model to describe the activated chemisorptions is Elovich equation. This model is useful for energetically heterogeneous solid surfaces [43]:

$$q_\mathrm{t} = \frac{1}{b}\ln(ab) + \frac{1}{b}\ln t \tag{17}$$

where a and b are constants. The constant a is considered as the initial sorption rate (mg/(g min)) and b is related to the extent of surface coverage and activation energy for chemisorptions (g mg^{-1}) and q_t (mg g^{-1}) is the amount of dye adsorbed at time t (min). The values of a and b obtained from the linear plots of q_t vs. ln t, are comprised in Table 2. Both initial sorption rate and extent of surface coverage increases with increase in temperature, insinuated that adsorption is favored at higher temperatures.

3.10.5. Bangham's equation

Kinetic data were further used to know about the slow step occurring in the present adsorption system using Bangham's equation [44].

$$\mathrm{Log}\,\log(C_\mathrm{o}/C_\mathrm{o} - q_\mathrm{t}m) = \log(k_\mathrm{o}m/2.303V) + \alpha\log t \tag{18}$$

where C_o is the initial concentration of dye in solution (mg L^{-1}). V is the volume of the solution (mL), m is the weight of adsorbent per liter of solution (g L^{-1}). q_t (mg g^{-1}) is amount of dye adsorbed at time t and α (<1) and k_o are constants and are accommodated in Table 2. Linear plot (Log log ($C_\mathrm{o}/C_\mathrm{o} - q_\mathrm{t}m$) vs. log t) demonstrated that the diffusion of adsorbate into pores of adsorbents is not the only rate-controlling step [45] The film and pore diffusion both were important to different extents in the removal process.

3.11. Activation parameters

Pseudo-second-order rate constant k_s was used to calculate the activation energy E_a for the adsorption of CV by EC using the Arrhenius equation:

$$\ln k_\mathrm{s} = \ln A - \frac{E_\mathrm{a}}{RT} \tag{19}$$

where k_s is the pseudo–second-order rate constant, A is the Arrhenius constant, E_a is the activation energy (kJ mol^{-1}), R is the gas constant (8.314 J mol^{-1} K^{-1}), and T is the temperature (K). The value of E_a was obtained from the slope of linear plot of ln k_s vs. $1/T$. The value of adsorption activation energy (E_a) was found to be 31.82 kJ mol^{-1}.

The Eyring equation was used to calculate the standard enthalpy ($\Delta H^{\#}$), and entropy of activation ($\Delta S^{\#}$) [46]:

$$\ln\frac{k_s}{T} = \ln\frac{k_B}{h} + \frac{\Delta S^{\#}}{R} - \frac{\Delta H^{\#}}{RT} \tag{20}$$

where k_s is the pseudo-second-order rate constant, k_B is the Boltzmann constant (1.3807×10^{-23} J K^{-1}), h is the Plank constant (6.6261×10^{-34} Js), R is the gas constant (8.314 J mol^{-1} K^{-1}) and T is the temperature (K). The values of $\Delta H^{\#}$ and $\Delta S^{\#}$ were calculated from the slope and intercept of the plot of ln (k_s/T) vs. $1/T$ was found to be 29.22 kJ mol^{-1} and −186.36 J mol^{-1} K^{-1}, respectively.

The values of $\Delta H^{\#}$ and $\Delta S^{\#}$ were used to compute the free energy of activation ($\Delta G^{\#}$) from the relation:

$$\Delta G^{\#} = \Delta H^{\#} - T\Delta S^{\#} \tag{21}$$

The value of $\Delta G^{\#}$ at 303, 313, and 323 K comes out to be 56.49, 58.35, and 60.22 kJ mol^{-1}, respectively. The large positive values of $\Delta G^{\#}$ suggest that energy was required in the adsorption process to convert reactants into products.

3.12. Error analysis

In recent decades, linear regression has been one of the most viable tools defining the best-fitting relationship quantifying the distribution of adsorbates, mathematically analyzing the adsorption systems and verifying the consistency and theoretical assumptions of an isotherm model. Due to the inherent bias resulting from linearization, five different error functions of nonlinear regression basin were employed in this study to find out the best-fit isotherm model to the experimental equilibrium data.

3.12.1. The sum of the squares of the errors

This error function, sum of the squares of the errors (SSE), is given as:

$$\mathrm{SSE} = \sum_{i=1}^{n} (q_{\mathrm{e,calc}} - q_{\mathrm{e,exp}})_i^2 \tag{22}$$

Here, $q_{\mathrm{e/cal}}$ and $q_{\mathrm{e/exp}}$ are, respectively, the calculated and the experimental value of the equilibrium adsorbate solid concentration in the solid phase (mg g^{-1}), and n is the number of data points. This is the most commonly used error function at higher end of the liquid-phase concentration ranges, the magnitude and squares of the errors tend to increase, illustrating a better fit for the isotherm parameters derivation [47].

3.12.2. The sum of the absolute errors

Sum of the absolute errors (SAE) is given as:

$$\mathrm{SAE} = \sum_{i=1}^{n} (|q_{\mathrm{e,calc}} - q_{\mathrm{e,exp}}|)_i \tag{23}$$

Isotherm parameters determined using the SAE method provides a better fit as the magnitude of the errors increases, biasing the fit towards the high concentration data [47].

3.12.3. The average relative error

The average relative error (ARE) is given as:

$$\mathrm{ARE} = \frac{100}{n} \sum_{i=1}^{n} \left| \frac{q_{\mathrm{e,calc}} - q_{\mathrm{e,exp}}}{q_{\mathrm{e,exp}}} \right|_i \tag{24}$$

ARE model that indicates a tendency to under or overestimate the experimental data, attempts to minimize the fractional error distribution across the entire studied concentration range [48].

3.12.4. The hybrid fractional error function

The hybrid fractional error function (HYBRID) is given as:

$$\mathrm{HYBRID} = \frac{100}{n-p} \sum_{i=1}^{n} \left[\frac{q_{\mathrm{e,calc}} - q_{\mathrm{e,exp}}}{q_{\mathrm{e,exp}}} \right]_i \tag{25}$$

This error function was developed [49] to improve the fit of the ARE method at low concentration values. Instead of n as used in ARE, the sum of the fractional errors is divided by $(n-p)$, where p is the number of parameters in the isotherm equation.

3.12.5. Marquardt's percent standard deviation (MPSD)

MPSD [50] has been used by a number of researchers in the field to test the adequacy and accuracy of the model fit with the experimental data. It has somewhat similarity to the geometric mean error distribu-

Table 3
Isotherm error analysis for adsorption of CV onto EC at different temperatures (adsorbent dose = 1 g L^{-1}, C_o = 20 mg L^{-1}, equilibrium time = 150 min, pH = 8)

Error function	SSE	SAE	ARE	HYBRID	MPSD
303 K					
Langmuir	0.31	1.13	1.78	−0.006	2.92
Freundlich	1.88	2.77	3.75	0.128	5.31
Tempkin	1.48	2.92	4.99	−0.95	7.98
D–R	0.45	1.41	1.93	−0.15	2.69
Generalized	24.53	12.11	19.77	24.35	27.33
313K					
Langmuir	0.089	0.65	0.87	−0.08	1.17
Freundlich	0.84	1.89	2.16	0.054	2.87
Tempkin	2.53	3.67	6.29	−0.93	10.23
D–R	0.089	0.68	0.89	0.002	1.16
Generalized	7.93	6.33	8.41	4.09	11.42
323K					
Langmuir	0.40	1.31	1.61	−0.02	2.43
Freundlich	0.24	1.14	1.39	0.024	1.77
Tempkin	5.81	6.03	9.26	−1.34	13.83
D–R	0.43	1.34	1.56	0.50	2.38
Generalized	11.85	7.54	9.20	−1.29	11.80

tion, but modified by incorporating the number of degrees of freedom. This error function is given as:

$$\mathrm{MPSD} = 100\sqrt{\frac{1}{n-p}\sum_{i=1}^{n}\left[\frac{(q_{\mathrm{e,exp}} - q_{\mathrm{e,calc}})}{q_{\mathrm{e,exp}}}\right]^2} \tag{26}$$

Table 3 shows that values of these error for the entire isotherm model. By comparing the results of the values of the error functions, it is found that the Langmuir isotherm best fits the CV adsorption isotherm data for the EC. Langmuir model best fits the removal of dye CV by EC at 303, 313, and 323 K.

3.13. Thermodynamic properties

The adsorption isotherm data obtained at different temperatures were used to calculate important thermodynamic parameters such as changes in Gibbs free energy ΔG, enthalpy change ΔH, and entropy change ΔS. The Langmuir constant, K_L (L mg^{-1}), was used to calculate changes in Gibbs free energy according to the following equations.

$$\Delta G = -RT \ln K_L \tag{27}$$

$$\Delta G = \Delta H - T\Delta S \tag{28}$$

ΔH and ΔS values were calculated from the slope and intercept of the plot of ln K_L vs. $1/T$ by linear regression method. The obtained ΔG values are −29.29, −30.12, and −31.93 kJ mol^{-1} at 303, 313, and 323 K, respectively. The value of ΔH and ΔS in the present study are evaluated as 9.16 kJ mol^{-1} and 127 $JK^{-1}mol^{-1}$, respectively. The positive values of ΔH for EC suggest that adsorption process is endothermic in nature and increase of temperature activates the adsorption sites. The positive value of ΔS indicates increase in the randomness in the system [51]. The negative values of ΔG reflected the feasibility and spontaneity of the adsorption process. The ΔG value becomes more negative with increasing temperature supports that CV adsorption on EC is favored with the increase in temperature.

4. Conclusion

- Results of adsorption under different experimental conditions corroborate that adsorption increases with increase in contact time, adsorbent dose, temperature, pH, and ionic strength.
- Characterization of adsorbent (EC) reveals the crystallite size 42.4 nm, particle size 51 μm, and BET surface area 23.6 m^2g^{-1}.
- Boehm titration indicated the basic nature of the adsorbent EC, which is further supported by the pH (8) value and pH_{ZPC}(7.9).

- The correlation coefficients (R^2) in the range of 0.9997–0.9998 and q_e values established that the second order kinetic model described the experimental sorption data.
- Langmuir model is found to be in good agreement with the experimental data on adsorptive behavior of the dye onto Eichhornia charcoal giving adorption capacity 58.1 mg g^{-1}. Results are also strengthened by the error functions.
- The values of Freundlich constant (K_F), Langmuir constant (K_L), monolayer concentration (C_m) D–R constant (q_s), Temkin constant (K_T), and initial sorption rate, "a" Elovich constant increases with increase in temperature, which demonstrate the endothermic nature of adsorption process. It is confirmed by the positive value of enthalpy change (ΔH) and activation parameters.
- The positive value of entropy change (ΔS) and negative value of free energy change (ΔG) indicated the increase of randomness and spontaneous nature of adsorption.
- The results alluded that the waste material Eichhornia can be fruitfully employed as a low cost material for the removal of CV from effluents of dye manufacturing and processing industries.

References

[1] A. Mittal, J. Mittal, A. Malviya, D. Kaur, V.K. Gupta, Adsorption of hazardous dye crystal violet from wastewater by waste materials, J. Colloid Interface Sci. 343 (2010) 463–473.

[2] C. Sahoo, A.K. Gupta, A. Pal, Photocatalytic degradation of crystal violet (C.I. Basic Violet 3) on silver ion doped TiO2, Dyes Pigm. 66 (2005) 189–196.

[3] R. Ahmad, Studies on adsorption of crystal violet dye from aqueous solution onto coniferous pinus bark powder (CPBP), J. Hazard Mater. 171 (2009) 767–773.

[4] A. Saeed, M. Sharif, M. Iqbal, Application potential of grapefruit peel as dye sorbent: Kinetics, equilibrium and mechanism of crystal violet adsorption, J. Hazard Mater. 179 (2010) 564–572.

[5] V.K. Gupta, I. Ali, T.A. Saleh, A. Nayak, S. Agarwal, Chemical treatment technologies for waste-water recycling—An overview, RSC Adv. 2 (2012) 6380–6388.

[6] V.K. Gupta, Suhas Application of low-cost adsorbents for dye removal—A review, J. Environ. Manage. 90 (2009) 2313–2342.

[7] L. Wang, Application of activated carbon derived from 'waste' bamboo culms for the adsorption of azo disperse dye: Kinetic, equilibrium and thermodynamic studies, J. Environ. Manage. 102 (2012) 79–87.

[8] P. Leechart, W. Nakbanpote, P. Thiravetyan, Application of 'waste' wood-shaving bottom ash for adsorption of azo reactive dye, J. Environ. Manage. 90 (2009) 912–920.

[9] A. Mittal, J. Mittal, L. Kurup, Utilization of hen feathers for the adsorption of a hazardous dye, indigo carmine from its simulated effluent, J. Environ. Prot. Sci. 1 (2007) 92–100.

[10] A. Mittal, D. Kaur, J. Mittal, Applicability of waste materials—Bottom ash and de-oiled soya, as adsorbents for the removal and recovery of a hazardous dye—Brilliant green, J. Colloid Interface Sci. 326 (2008) 8–17.

[11] A. Mittal, D. Kaur, J. Mittal, Batch and bulk removal of a triarylmethane dye—Fast green FCF, from wastewater by adsorption over waste materials, J. Hazard Mater. 163 (2009) 568–577.

[12] A. Mittal, R. Jain, S. Varshney, S. Sikarwar, J. Mittal, Removal of yellow me 7 gl from industrial effluent using electrochemical and adsorption techniques, Int. J. Environ. Pollut. 43(4) (2010) 308–323.

[13] A. Mittal, R. Jain, J. Mittal, M. Shrivastava, Adsorptive removal of hazardous dye quinoline yellow from waste water using coconut-husk as potential adsorbent, Fresenius Environ. Bull. 19(6) (2010) 1–9.

[14] A. Mittal, D. Jhare, J. Mittal, V.K. Gupta, Batch and bulk removal of hazardous colouring agent rose Bengal by adsorption over bottom ash, RSC Adv. 2(22) (2012) 8381–8389.

[15] A. Mittal, V. Thakur, V. Gajbe, Evaluation of adsorption characteristics of an anionic azo dye brilliant yellow onto hen feathers in aqueous solutions, Environ. Sci. Pollut. Res. 19(6) (2012) 2438–2447.

[16] H. Daraei, A. Mittal, J. Mittal, H. Kamali, Optimization of Cr(VI) removal onto biosorbent eggshell membrane: Experimental & theoretical approaches, Desalin. Water Treat. (2013), doi: 10.1080/19443994.2013.787374.

[17] J. Mittal, D. Jhare, H. Vardhan, A. Mittal, Utilization of bottom ash as a low-cost sorbent for the removal and recovery of a toxic halogen containing dye eosin yellow, Desalin. Water Treat. (2013), doi: 10.1080/19443994.2013.803265.

[18] G. Crini, Non-conventional low-cost adsorbents for dye removal: A review, Bioresour. Technol. 97 (2006) 1061–1085.

[19] I. Ali, M. Asim, T.A. Khan, Low cost adsorbents for the removal of organic pollutants from wastewater, J. Environ. Manage. 113 (2012) 170–183.

[20] A. Malik, Environmental challenge vis a vis opportunity: The case of water hyacinth, Environ. Int. 33 (2007) 122–138.

[21] L. Lachman, H.A. Lieberman, The Theory and Practice of Industrial Pharmacy, CBS Publishers, Delhi, 2009, p. 27.

[22] J. Rivera-Utrilla, I. Bautista-Toledo, M.A. Ferro-Garcia, C. Moreno-Castilla, Activated carbon surface modifications by adsorption of bacteria and their effect on aqueous lead adsorption, J. Chem. Technol. Biotechnol. 76 (2001) 1209–1215.

[23] H.P. Boehm, Some aspects of the surface chemistry of carbon blacks and other carbons, Carbon 32 (1994) 759–769.

[24] B.D. Cullity, Elements of X-ray Diffraction, Addison-Wesley Publishing Company, Boston, MA, 1956, p. 261.

[25] P. Prema, S. Thangapandian, M. Selvarani, S. Subharanjani, C. Amutha, Color removal efficiency of dyes using nano zero valent iron treatment, Toxicol. Environ. Chem. 93(10) (2011) 1908–1917.

[26] I.D. Mall, V.C. Srivastava, G.V.A. Kumar, I.M. Mishra, Characterization and utilization of mesoporous fertilizer plant waste carbon for adsorptive removal of dyes from aqueous solution, Colloids Surf., A 278(1–3) (2006) 175–187.

[27] P.D. Saha, S. Chakraborty, S. Chowdhury, Batch and continuous (fixed-bed column) biosorption of crystal violet by *Artocarpus heterophyllus* (jackfruit) leaf powder, Colloids Surf., B 92 (2012) 262–270.

[28] S.D. Khattri, M.K. Singh, Use of sagaun sawdust as an adsorbent for the removal of crystal violet dye from simulated wastewater, Environ. Prog. Sustainable Energy 31(3) (2012) 435–442.

[29] S.A. Cardenas, S.L. Cortez, M.C. Mazon, J.C.M. Gutierrez, Study of malachite green adsorption by organically modified clay using a batch method, Appl. Surf. Sci. 280 (2013) 74–78.

[30] M. Ozacar, I.A. Sengil, Adsorption of metal complex dyes from aqueous solutions by pine sawdust, Bioresour. Technol. 96 (2005) 791–795.

[31] A. Shukla, Y.H. Zhang, P. Dubey, J.L. Margrave, S.S. Shukla, The role of sawdust in the removal of unwanted materials from water, J. Hazard. Mater. B 95 (2002) 137–152.

[32] L.J. Yu, S.S. Shukla, K.L. Dorris, A. Shukla, J.L. Margrave, Adsorption of chromium from aqueous solutions by maple sawdust, J. Hazard. Mater. B 100 (2003) 53–63.

[33] G. Newcombe, M. Drikas, Adsorption of NOM activated carbon: Electrostatic and non-electrostatic effects, Carbon 35 (1997) 1239–1250.

[34] G. Alberghina, R. Bianchini, M. Fichera, S. Fisichella, Dimerization of cibacron blue F3GA and other dyes: Influence of salts and temperature, Dyes Pigm. 46 (2000) 129–137.

[35] V.S. Mane, I.D. Mall, V.C. Srivastava, Kinetic and equilibrium isotherm studies for the adsorptive removal of brilliant green dye from aqueous solution by rice husk ash, J. Environ. Manage. 84 (2007) 390–400.

[36] Y.S. Ho, J.F. Porter, G. McKay, Equilibrium isotherm studies for the sorption of divalent metal ions onto peat: Copper, nickel and lead single component systems, Water Air Soil Pollut. 141 (2002) 1–33.

[37] A. Mittal, J. Mittal, A. Malviya, V.K. Gupta, Adsorptive removal of hazardous anionic dye ‘‘congo red” from wastewater using waste materials and recovery by desorption, J. Colloid Interface Sci. 340 (2009) 16–26.

[38] F. Kargi, S. Ozmihci, Biosorption performance of powdered activated sludge for removal of different dyestuff, Enzyme Microb. Technol. 35 (2004) 267–271.

[39] M.J. Weber, J. Morris, Kinetic of adsorption on carbon from solution, J. Sanit. Eng. Div. ASCE 89 (1963) 31–59.

[40] U.R. Lakshmi, V.C. Srivastava, I.D. Mall, D.H. Lataye, Rice husk ash as an effective adsorbent: Evaluation of adsorptive characteristics for indigo carmine dye, J. Environ. Manage. 90 (2009) 710–720.

[41] G.E. Boyd, A.W. Adamson, L.S. Meyers, The exchange adsorption of ions from aqueous solution by organic zeolites II kinetics, J. Am. Chem. Soc. 69 (1947) 2836–2848.

[42] S. Wang, H. Li, L. Xu, Application of zeolite MCM-22 for basic dye removal from wastewater, J. Colloid Interface Sci. 295 (2006) 71–78.

[43] M. Ozacar, I.A. Sengil, A kinetic study of metal complex dye sorption onto pine sawdust, Process Biochem. 40 (2005) 565–572.

[44] C. Aharoni, S. Sideman, E. Hoffer, Adsorption of phosphate ions by colloid ion—Coated alumina, J. Chem. Technol. Biotechnol. 29 (1979) 404–412.

[45] E. Tutem, R. Apak, C.F. Unal, Adsorptive removal of chlorophenols from water by bituminous shale, Water Res. 32 (1998) 2315–2324.

[46] S. Chowdhury, P. Saha, Sea shell powder as a new adsorbent to remove basic green 4 (malachite green) from aqueous solutions: Equilibrium kinetic and thermodynamic studies, Chem. Eng. J**.** 164 (2010) 168–177.

[47] S. Chowdhury, R. Mishra, P. Saha, P. Kushwaha, Adsorption thermodynamics kinetics and isosteric heat of adsorption of malachite green onto chemically modified rice husk, Desalination 265 (2011) 159–168.

[48] R.K. Rajoriya, B. Prasad, I.M. Mishra, K.L. Wasewar, Adsorption of benzaldehyde on granular activated carbon: Kinetics, equilibrium, and thermodynamic, Chem. Biochem. Eng. Q. 21 (3) (2007) 219–226.

[49] A. Kapoor, R.T. Yang, Correlation of equilibrium adsorption data of condensible vapours on porous adsorbents, Gas Sep. Purif. 3(4) (1989) 187–192.

[50] J.F. Porter, G. Mckay, K.H. Choy, The prediction of sorption from a binary mixture of acidic dyes using single- and mixed-isotherm variants of the ideal adsorbed solute theory, Chem. Eng. Sci. 54 (1999) 5863–5885.

[51] K. Vijayaraghavan, Y.S. Yun, Biosorption of C.I reactive black 5 from aqueous solution using acid–treated biomass of brown seaweed laminaria sp, Dyes Pigm. 76 (2008) 726–732.